# Ultrafast Spontaneous Emission from a Slot-Antenna Coupled $WSe_2$ Monolayer

Michael S. Eggleston,[†,‡] Sujay B. Desai,[†,§] Kevin Messer,[†] Seth A. Fortuna,[†] Surabhi Madhvapathy,[†,§] Jun Xiao,[∥] Xiang Zhang,[§,∥] Eli Yablonovitch,[†] Ali Javey,[†,§] and Ming C. Wu*[,†]

[†]Electrical Engineering and Computer Sciences, University of California, Berkeley, California 94720, United States
[§]Materials Sciences Division, Lawrence Berkeley National Laboratory, Berkeley, California 94720, United States
[∥]Nanoscale Science and Engineering Center, University of California, Berkeley, California 94720, United States

Supporting Information

**ABSTRACT:** Optical antennas can enhance the spontaneous emission rate from nanoemitters by orders of magnitude, enabling the possibility of an ultrafast, efficient, nanoscale LED. Semiconductors would be the preferred material for such a device to allow for direct high-speed modulation. However, efficient nanoscale devices are challenging to implement because of high surface recombination typical of most III–V materials. Monolayer transition metal dichalcogenides are an attractive alternative to a III–V emitter due to their intrinsically nanoscale dimensions, direct bandgap, and near-ideal surfaces resulting in high intrinsic quantum yield. In this work, we couple a nanostrip (30 nm × 250 nm) monolayer of $WSe_2$ to a cavity-backed optical slot antenna through a self-aligned fabrication process. Photoluminescence, scattering, and lifetime measurements are used to estimate a radiative spontaneous emission rate enhancement of 318× from $WSe_2$ monolayers coupled to on-resonance antennas. Such a huge increase in the spontaneous emission rate results in an ultrafast radiative recombination rate and a quantum yield in nanopatterned monolayers comparable to unprocessed exfoliated flakes of $WSe_2$.

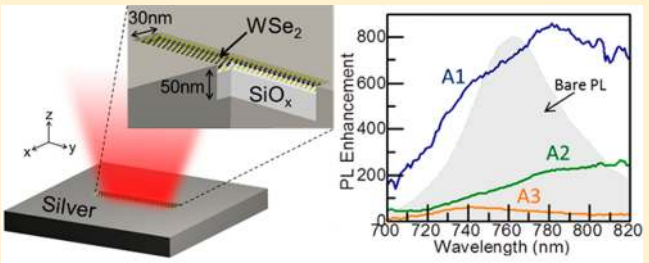


**KEYWORDS:** *optical antenna, nanoLED, 2D materials, metal optics, nanophotonics, plasmonics*

Optical antennas have demonstrated an enormous ability to focus free-space optical energy down to nanoscale dimensions as well as radiate locally stored energy into the far-field. Plasmonic structures and optical antennas have been shown to enhance absorption,[1,2] Raman scattering,[3,4] and spontaneous emission rates of nanoemitters[5−12] by orders of magnitude. Increasing spontaneous emission rates is especially attractive as it could enable efficient LEDs with modulation bandwidths exceeding that of traditional directly modulated lasers,[13] leading to a new class of devices for on-chip optical interconnects and nanoscale optical sensors. Spontaneous emission rate enhancement has been successful for dye-molecule emission,[5,7−9] where high intrinsic quantum yield and simple fabrication methods allow for tight coupling between the dye-molecule and optical antenna. Dye-molecules, however, can only be excited optically and have a slow response time that severely limits their use as integrated nanoemitters that require direct modulation at high speed. Coupling solid-state emitters to optical antennas has also been extensively studied,[6,10,11,14] but these attempts have shown significantly lower enhancement and quantum yield than their dye-molecule counterparts. In solid-state emitters at the nanoscale, surface recombination plays a significant role. To maintain a high quantum yield, cladding layers must be utilized to prevent carriers from reaching the surface. These cladding layers, however, prevent the emitter from being closely coupled to an optical antenna, creating an intrinsic trade-off between rate enhancement and device quantum efficiency.

Transition metal dichalcogenide (TMDC) materials such as $MoS_2$ and $WSe_2$ have emerged as an interesting new optoelectronic material.[15−24] Monolayers exhibit a direct bandgap and offer near ideal surfaces, resulting in high intrinsic photoluminescence quantum yield.[16,25] These unique properties, along with the ability to electrically inject carriers,[26] have allowed for a wide range of optoelectronic devices to be demonstrated with TMDCs including LEDs,[27−29] solar cells,[30] and photodetectors.[31] Their strong light emission, near-ideal surfaces, and intrinsically atomic layer thickness make TMDCs very attractive candidates for use in an optical nanoemitter.

By using $WSe_2$ as the active material in an optical antenna based nanoLED, we demonstrate photoluminescence (PL) enhancement as large as 700× compared to bare monolayers. Unlike previous studies that aimed solely at increasing PL, whether through a pump enhancement, increased directivity, or radiative decay rate enhancement,[32−34] our structures are specifically designed to enhance radiative decay rate. Radiative decay rate defines the fastest speed at which energy can escape

**Received:** March 25, 2018
**Published:** June 6, 2018

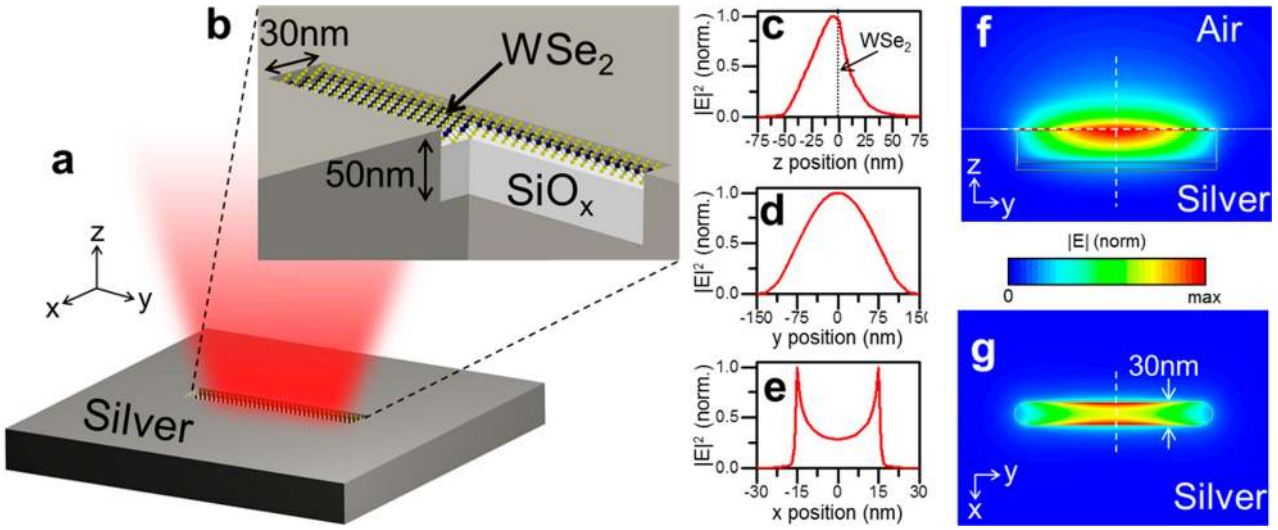


**Figure 1.** (a) Perspective view of cavity-backed slot antenna. (b) Perspective cut-through schematic of $WSe_2$ monolayer coupled to an optical slot antenna. (c) $|E|^2$ in the $z$-direction at $x = y = 0$. (d) $|E|^2$ through the center of the $WSe_2$ layer along the $y$-direction and (e) along the $x$-direction. (f) Cut-plane along the slot long axis and (f) through the $WSe_2$ layer showing the electric-field profile of the antenna mode. White dotted lines correspond to the $|E|^2$ profiles in (c–e).

from a material into free space as photons and is therefore the ultimate limiting factor in speed and efficiency of a high-speed modulated LED. PL, scattering, and lifetime measurements of our devices suggest that in devices where the antenna resonance is well matched to the $WSe_2$ spontaneous emission spectrum, the rate of radiative emission is enhanced by a factor of 318× compared to bare etched $WSe_2$ monolayers. To the best of our knowledge, this is the largest rate enhancement ever reported for any semiconductor emitter. Such a large rate enhancement compensates for increased nonradiative edge recombination[35] present in nanoscale flakes (~30 nm × 250 nm), resulting in antenna-coupled devices with a quantum yield comparable to unprocessed monolayers. The combination of ultrafast radiative lifetime and high quantum yield make this structure an attractive option for future high-speed directly modulated nanoemitters.

In this work, we couple $WSe_2$ nanoemitters to optical slot antennas as shown in Figure 1a. The slot antenna is the complementary structure to the dipole antenna,[36] formed by creating a dielectric slot in a continuous metal plane. The dipole antenna and slot antenna have very similar far-field radiation characteristics, but have significantly different near-field. The electric field of a slot antenna, shown in Figure 1f,g for the structure used in this study, is concentrated within the dielectric slot, which provides an effective way to couple to a dipole emitter. A cavity-backed slot antenna[12,37] is a slight perturbation of the slot antenna that closes off the back side of the slot with a metal reflector. This creates an antenna that directionally emits in the $+z$ direction and eliminates the need for fine lithographic alignment of the active material and the antenna. By using a self-aligned fabrication process, $WSe_2$ not within the slot of the antenna is completely etched away (see Supporting Information). This ensures tight coupling between the semiconductor and antenna without the need for tight fabrication tolerances and eliminates background material that would otherwise be poorly coupled to the antenna. In our experiment, very coarse alignment was used to pattern antennas in the portion of the substrate containing monolayer $WSe_2$.

Continuous-wave (CW) PL, time-resolved PL, and white light scattering measurements were performed to experimentally measure the emission properties of the antennas. Collected optical emission from three different antenna-coupled devices and a bare reference sample are shown in Figure 3. Antennas

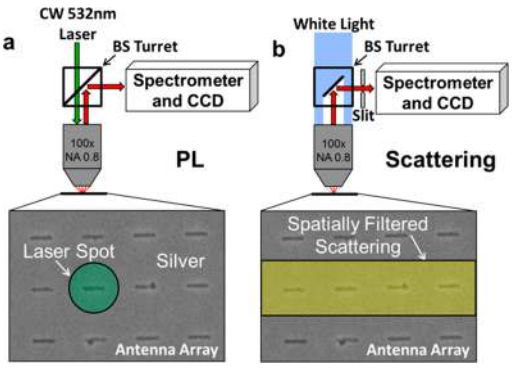


**Figure 2.** (a) Experimental PL measurement setup. Laser spot size is approximately equal to the antenna spacing, 700 nm, allowing individual antennas to be probed at a time. (b) The setup can be converted to scattering measurement by rotating a beam splitter turret. The scattering from an entire row of antennas is measured at a time on a two-dimensional CCD, allowing for the spectrum of each individual antenna to be determined.

are resonant structures and therefore have a limited bandwidth at which they can efficiently operate, defined by their quality factor ($Q$). Ideally, we want an antenna with high radiation losses and therefore with very low $Q$, on the order of ~1. The slot antenna structure used has a $Q$ of ~12, as discussed in the Supporting Information, and therefore has a limited bandwidth that must be matched to the emission wavelength of $WSe_2$. The measured devices are from different samples whose (A1) antenna resonances are closely matched to the emission wavelength of $WSe_2$, (A2) red-shifted from the peak emission, and (A3) far off resonance. This was accomplished by changing the dimensions (width × length × height) of the $SiO_x$ slot for the different devices as follows: A1 was 30 nm × 250 nm × 40 nm, A2 was 30 nm × 300 nm × 40 nm, A3 was 30 nm × 300 nm × 32 nm, and the bare sample was 30 nm × 300 nm. These

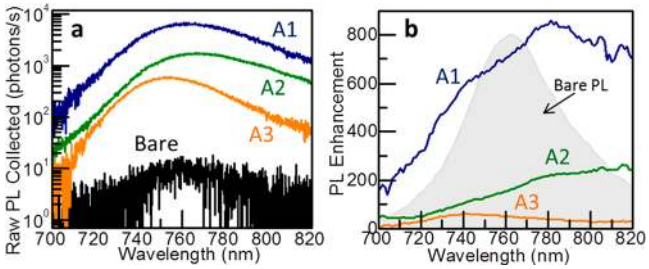


**Figure 3.** (a) Raw number of photons per second collected for devices A1 (blue), A2 (green), and A3 (orange) compared to a bare (black) etched WSe2 monolayer. (b) Enhanced PL from three antenna-coupled devices calculated by taking the ratio of the results in (a) by the emission from a bare etched mononlayer. The shaded gray curve shows the PL spectrum of the bare monolayer.

three devices exhibit a raw PL enhancement compared to the bare sample averaged over the full optical spectrum of 700×, 190×, and 47×, respectively. This large increase in PL can be attributed to three factors: enhanced collection efficiency, enhanced pumping, and enhanced quantum yield due to an increased spontaneous emission rate. To determine the difference in collection efficiency between the bare and antenna-coupled devices, 3D time domain simulations (CST Microwave Studio) were performed to calculate their far-field emission patterns. Simulations show bare etched samples have a collection efficiency into a NA = 0.8 objective of 17.2% compared to 48% for an antenna-coupled device. The antenna therefore provides a 2.8× increase in collection efficiency.

To remove the possibility of large pump enhancements, scattering measurements are used to ensure the antenna resonance is close to the emission wavelength and far from the pump wavelength. The same optical setup, shown in Figure 2, is used to measure scattering and PL (see Methods). Figure 4

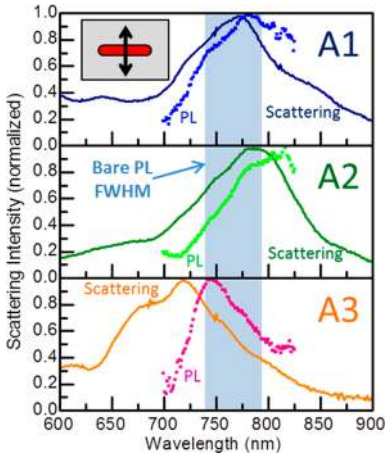


**Figure 4.** Measured scattering spectra of three different antennas with light polarized perpendicular to the slot. Normalized PL enhancement is plotted as colored squares. The full-width half-maximum of the bare PL spectrum is highlighted in blue.

shows the scattering intensity of light polarized in the antenna polarization compared to the normalized PL enhancement for each antenna. Although the scattering is spatially filtered with a narrow slit, the scattering from neighboring antennas is not completely eliminated due to the close 700 nm spacing of each antenna. The scattering can therefore only give us a qualitative measurement of the antenna resonance frequency and spectral shape. Regardless, the shape of the PL enhancement follows very closely to the scattering spectrum for the three devices. The resonance of A1 overlaps the emission spectra nicely and has the highest PL enhancement. Device A2 has a scattering spectrum slightly red-shifted from the emission spectra and correspondingly its PL is weaker than device A1. Finally, the resonance wavelength of A3 is very blue-shifted from the emission spectra which accounts for its much weaker PL emission.

The scattering spectra of light polarized parallel to the slot (and therefore parallel to the pump laser) of all three devices is fairly flat across all wavelengths (see Supporting Information), indicating a lack of resonant pump enhancement. The effect of the metal antenna on off-resonance pump conditions was simulated using 3D simulations (CST Microwave Studio, COMSOL) by measuring the local field intensity in the $WSe_2$ layer as a function of plane wave excitation wavelength. Because the laser pump is polarized perpendicular to the antenna resonance mode, very little enhancement is observed. Simulations predict a 1.6× pump enhancement for antenna coupled devices versus bare etched flakes. Similar to the measured scattering of devices A1−A3, the simulated pumping is far off resonance and is very minimally affected by minor changes in the slot height and length.

With an understanding of the enhanced extraction efficiency and pumping, the last source of PL enhancement is increased quantum yield. Light emitted per unit area from the bare etched sample is 2 orders of magnitude weaker than the brightest unprocessed bare flakes. Unprocessed WSe2 has a quantum yield of ∼1%,[26] which would give the bare etched sample a quantum yield closer to 1e-4. This signifies that the edges exposed during the etch process significantly increase the nonradiative recombination rates as previously reported.[35] Since the same etching process is used for all samples, this pins the total recombination rate of all the devices at the same edge-recombination limited rate (∼1 ps measured by streak camera; see Supporting Information). Edge passivation or heterojunction cladding could potentially increase the quantum yield of future devices,[38,39] but for this study, the edges are left unpassivated so that an increase in quantum yield is a measure of the enhanced spontaneous emission rate. Since only the dipole moments in the $WSe_2$ oriented perpendicular to the slot long-axis will couple to the antenna, increased quantum yield is only caused by a spontaneous emission rate increase in half the total dipoles in the material.

Combining the factors for increased collection efficiency, enhanced pumping, and the contribution of only half the dipole moments in the material gives a total adjustment factor of 2.2×. The increased PL emission from the antenna-coupled devices therefore corresponds to an estimated rate increase of 318×, 86×, and 21× for devices A1, A2, and A3, respectively. This huge increase in spontaneous emission makes the overall quantum yield of our best devices comparable to unprocessed monolayers.

The simulated enhancement provided by the cavity-backed slot antenna into the far-field is 420× with an antenna efficiency of 54%, although the enhancement is highly dependent on the exact width of the slot (see Supporting Information). The slightly lower rate enhancements observed experimentally can be explained by a mismatch between antenna resonance and PL spectrum, small deviations in the slot width from the 30 nm simulated, and decreased antenna efficiency from less than ideal silver quality. Using a simple circuit model, we can estimate that

even a small ∼6% drop in antenna efficiency from nonideal silver quality can drop the maximum expected rate enhancement to 318× (see Supporting Information).

In conclusion, we have demonstrated an etched nanostrip of monolayer $WSe_2$ coupled to a silver cavity-backed slot antenna. PL enhancements up to 700× from nonresonantly pumped structures were measured with estimated spontaneous emission rate enhancements as high as 318×. Future work to passivate or clad the detrimental edges could increase the quantum yield of the device to near unity. Such an ultrafast and efficient nanoscale semiconductor emitter is an ideal choice for future directly modulated nanoscale light sources. This new class of nanoemitter would have significant impacts on short-range communication and nanoscale sensing by enabling modulation rates and power efficiencies unobtainable in traditional light-emitting devices.

## METHODS

Devices are fabricated by first mechanically exfoliating $WSe_2$ flakes onto a 260 nm thick $Si/SiO_2$ substrate and transferring them onto a disposable carrier substrate. A 40 nm thick $SiO_x$ layer is then deposited followed by a thin chrome hardmask that is patterned to define the width and length of the dielectric slot. The chrome masks the $SiO_x$ in an $SF_6$-based reactive ion etch that also etches through the $WSe_2$ monolayer below and defines the slot. For antenna-coupled devices, the slot is covered in a blanket silver evaporation. This step is skipped for bare reference devices. The whole chip is then bonded to a glass carrier wafer with UV epoxy and the carrier substrate is completely removed to allow for topside collection and eliminate light trapping effects. The final structure, shown in Figure 1a, consists of a 50 nm deep slot 30 nm wide and 250 nm long in a silver plane. At the very top of the slot is the etched $WSe_2$ active region. The entire structure is coated with an $Al_2O_3$ layer to prevent silver oxidation. Detailed fabrication steps are given in the Supporting Information.

CW PL measurements are performed by generating carriers in the $WSe_2$ with a 532 nm CW laser polarized parallel to the slot with a $\mu$-PL microscope system, shown in Figure 2a. Optical emission is collected with a 0.8 NA 100× objective, passed through a spectrometer and readout on a Princeton Instruments liquid nitrogen cooled silicon CCD. The laser spot size is the same as the antenna pitch, 700 nm, which allows single devices to be probed. By rotating a beam splitter (BS) turret in the microscope the system can be configured for scattering measurements (Figure 2b). This allows the PL and scattering response of each individual antenna to be measured and directly compared. Scattering measurements are performed by illuminating the dark-field illumination ring on the back-aperture of the microscope objective with white light. The dark-field illumination ring then focuses the white light onto the sample at angles larger than the collection angle of the objective. Specular reflection off of the sample is therefore at angles too large for the objective to collect and only antenna-backscatter at smaller angles can be collected. Collected light is then focused onto a slit at the input of the spectrometer which narrows the field-of-view to a single line of antennas, as shown in Figure 2b. The spectrometer disperses the light onto a 2D CCD so that the intensity of backscatter versus wavelength can be read-off for each antenna in the single line.

## ASSOCIATED CONTENT

### Supporting Information

Lifetime measurements of unprocessed and antenna coupled $WSe_2$ monolayers; detailed fabrication methods; simulated rate enhancement and efficiency; circuit model derivation of rate enhancement and efficiency; defects in antenna samples; and white light scattering measurements of light polarized parallel to the antenna (PDF).

## AUTHOR INFORMATION


### Corresponding Author

*E-mail: wu@eecs.berkeley.edu.

### ORCID

Michael S. Eggleston: 0000-0002-2255-4966
Jun Xiao: 0000-0003-4248-8190
Xiang Zhang: 0000-0002-3272-894X
Ali Javey: 0000-0001-7214-7931

### Present Address

‡Nokia Bell Laboratories, Murray Hill, New Jersey 07974, United States.



### Funding

National Science Foundation (NSF) Center for Energy Efficient Electronics Science (E3S) Award ECCS-0939514; AFOSR Award FA9550-09-1-0598.

### Notes

The authors declare no competing financial interest.


## REFERENCES


(1) Tang, L.; Kocabas, S. E.; Latif, S.; Okyay, A. K.; Ly-Gagnon, D.-S.; Saraswat, K. C.; Miller, D. A. B. Nanometre-Scale Germanium Photodetector Enhanced by a near-Infrared Dipole Antenna. *Nat. Photonics* **2008**, *2*, 226−229.

(2) Najmaei, S.; Mlayah, A.; Arbouet, A.; Girard, C.; Léotin, J.; Lou, J. Plasmonic Pumping of Excitonic Photoluminescence in Hybrid $MoS_2$ − Au Nanostructures. *ACS Nano* **2014**, *8* (12), 12682−12689.

(3) Zhu, W.; Banaee, M. G.; Wang, D.; Chu, Y.; Crozier, K. B. Lithographically Fabricated Optical Antennas with Gaps Well Below 10 Nm. *Small* **2011**, *7* (13), 1761−1766.

(4) Seok, T. J.; Jamshidi, A.; Eggleston, M.; Wu, M. C. Mass-Producible and Efficient Optical Antennas with CMOS-Fabricated Nanometer-Scale Gap. *Opt. Express* **2013**, *21* (14), 16561−16569.

(5) Kinkhabwala, A.; Yu, Z.; Fan, S.; Avlasevich, Y.; Mullen, K.; Moerner, W. E. Large Single-Molecule Fluorescence Enhancements Produced by a Bowtie Nanoantenna. *Nat. Photonics* **2009**, *3* (11), 654−657.

(6) Eggleston, M. S.; Messer, K.; Zhang, L.; Yablonovitch, E.; Wu, M. C. Optical Antenna Enhanced Spontaneous Emission. *Proc. Natl. Acad. Sci. U. S. A.* **2015**, *112*, 1704.

(7) Lee, K.-G.; Eghlidi, H.; Chen, X.-W.; Renn, A.; Götzinger, S.; Sandoghdar, V. Spontaneous Emission Enhancement of a Single Molecule by a Double-Sphere Nanoantenna across an Interface. *Opt. Express* **2012**, *20* (21), 23331.

(8) Zhang, W.; Ding, F.; Li, W.-D.; Wang, Y.; Hu, J.; Chou, S. Y. Giant and Uniform Fluorescence Enhancement over Large Areas Using Plasmonic Nanodots in 3D Resonant Cavity Nanoantenna by Nanoimprinting. *Nanotechnology* **2012**, *23* (22), 225301.

(9) Akselrod, G. M.; Argyropoulos, C.; Hoang, T. B.; Ciracì, C.; Fang, C.; Huang, J.; Smith, D. R.; Mikkelsen, M. H. Probing the Mechanisms of Large Purcell Enhancement in Plasmonic Nanoantennas. *Nat. Photonics* **2014**, *8*, 835.

(10) Arbel, D.; Berkovitch, N.; Nevet, A.; Peer, A.; Cohen, S.; Ritter, D.; Orenstein, M. Light Emission Rate Enhancement from InP MQW by Plasmon Nano-Antenna Array. *Opt. Express* **2011**, *19* (10), 9807.
(11) Huang, K. C. Y.; Seo, M.-K.; Huo, Y.; Sarmiento, T.; Harris, J. S.; Brongersma, M. L. Antenna Electrodes for Controlling Electroluminescence. *Nat. Commun.* **2012**, *3*, 1005.
(12) Song, J.-H.; Kim, J.; Jang, H.; Yong Kim, I.; Karnadi, I.; Shin, J.; Shin, J. H.; Lee, Y.-H. Fast and Bright Spontaneous Emission of $Er^{3+}$ Ions in Metallic Nanocavity. *Nat. Commun.* **2015**, *6*, na.
(13) Lau, E. K.; Lakhani, A.; Tucker, R. S.; Wu, M. C. Enhanced Modulation Bandwidth of Nanocavity Light Emitting Devices. *Opt. Express* **2009**, *17* (10), 7790.
(14) Farahani, J. N.; Pohl, D. W.; Eisler, H.-J.; Hecht, B. Single Quantum Dot Coupled to a Scanning Optical Antenna: A Tunable Superemitter. *Phys. Rev. Lett.* **2005**, *95* (1), na.
(15) Novoselov, K. S.; Jiang, D.; Schedin, F.; Booth, T. J.; Khotkevich, V. V.; Morozov, S. V.; Geim, A. K. Two-Dimensional Atomic Crystals. *Proc. Natl. Acad. Sci. U. S. A.* **2005**, *102* (30), 10451−10453.
(16) Mak, K. F.; Lee, C.; Hone, J.; Shan, J.; Heinz, T. F. Atomically Thin $MoS_2$: A New Direct-Gap Semiconductor. *Phys. Rev. Lett.* **2010**, *105* (13), na.
(17) Wang, Q. H.; Kalantar-Zadeh, K.; Kis, A.; Coleman, J. N.; Strano, M. S. Electronics and Optoelectronics of Two-Dimensional Transition Metal Dichalcogenides. *Nat. Nanotechnol.* **2012**, *7* (11), 699−712.
(18) Peimyoo, N.; Shang, J.; Cong, C.; Shen, X.; Wu, X.; Yeow, E. K. L.; Yu, T. Nonblinking, Intense Two-Dimensional Light Emitter: Monolayer $WS_2$ Triangles. *ACS Nano* **2013**, *7* (12), 10985−10994.
(19) Radisavljevic, B.; Radenovic, A.; Brivio, J.; Giacometti, V.; Kis, A. Single-Layer MoS2 Transistors. *Nat. Nanotechnol.* **2011**, *6* (3), 147−150.
(20) Fang, H.; Chuang, S.; Chang, T. C.; Takei, K.; Takahashi, T.; Javey, A. High-Performance Single Layered WSe2 P-FETs with Chemically Doped Contacts. *Nano Lett.* **2012**, *12* (7), 3788−3792.
(21) Butler, S. Z.; Hollen, S. M.; Cao, L.; Cui, Y.; Gupta, J. A.; Gutiérrez, H. R.; Heinz, T. F.; Hong, S. S.; Huang, J.; Ismach, A. F.; et al. Progress, Challenges, and Opportunities in Two-Dimensional Materials Beyond Graphene. *ACS Nano* **2013**, *7* (4), 2898−2926.
(22) Chhowalla, M.; Shin, H. S.; Eda, G.; Li, L.-J.; Loh, K. P.; Zhang, H. The Chemistry of Two-Dimensional Layered Transition Metal Dichalcogenide Nanosheets. *Nat. Chem.* **2013**, *5* (4), 263−275.
(23) Xu, M.; Liang, T.; Shi, M.; Chen, H. Graphene-Like Two-Dimensional Materials. *Chem. Rev.* **2013**, *113* (5), 3766−3798.
(24) Jariwala, D.; Sangwan, V. K.; Lauhon, L. J.; Marks, T. J.; Hersam, M. C. Emerging Device Applications for Semiconducting Two-Dimensional Transition Metal Dichalcogenides. *ACS Nano* **2014**, *8* (2), 1102−1120.
(25) Zhao, W.; Ghorannevis, Z.; Chu, L.; Toh, M.; Kloc, C.; Tan, P.-H.; Eda, G. Evolution of Electronic Structure in Atomically Thin Sheets of $WS_2$ and $WSe_2$. *ACS Nano* **2013**, *7* (1), 791−797.
(26) Lien, D.-H.; Amani, M.; Desai, S. B.; Ahn, G. H.; Han, K.; He, J.-H.; Ager, J. W.; Wu, M. C.; Javey, A. Large-Area and Bright Pulsed Electroluminescence in Monolayer Semiconductors. *Nat. Commun.* **2018**, *9* (1), na.
(27) Ross, J. S.; Klement, P.; Jones, A. M.; Ghimire, N. J.; Yan, J.; Mandrus, D. G.; Taniguchi, T.; Watanabe, K.; Kitamura, K.; Yao, W.; et al. Electrically Tunable Excitonic Light-Emitting Diodes Based on Monolayer WSe2 P-N Junctions. *Nat. Nanotechnol.* **2014**, *9* (4), 268−272.
(28) Jo, S.; Ubrig, N.; Berger, H.; Kuzmenko, A. B.; Morpurgo, A. F. Mono- and Bilayer $WS_2$ Light-Emitting Transistors. *Nano Lett.* **2014**, *14* (4), 2019−2025.
(29) Cheng, R.; Li, D.; Zhou, H.; Wang, C.; Yin, A.; Jiang, S.; Liu, Y.; Chen, Y.; Huang, Y.; Duan, X. Electroluminescence and Photocurrent Generation from Atomically Sharp $WSe_2$ /$MoS_2$ Heterojunction *P*−*n* Diodes. *Nano Lett.* **2014**, *14* (10), 5590−5597.
(30) Pospischil, A.; Furchi, M. M.; Mueller, T. Solar-Energy Conversion and Light Emission in an Atomic Monolayer P−n Diode. *Nat. Nanotechnol.* **2014**, *9* (4), 257−261.
(31) Lopez-Sanchez, O.; Lembke, D.; Kayci, M.; Radenovic, A.; Kis, A. Ultrasensitive Photodetectors Based on Monolayer MoS2. *Nat. Nanotechnol.* **2013**, *8* (7), 497−501.
(32) Butun, S.; Tongay, S.; Aydin, K. Enhanced Light Emission from Large-Area Monolayer $MoS_2$ Using Plasmonic Nanodisc Arrays. *Nano Lett.* **2015**, *15*, 2700.
(33) Akselrod, G. M.; Ming, T.; Argyropoulos, C.; Hoang, T. B.; Lin, Y.; Ling, X.; Smith, D. R.; Kong, J.; Mikkelsen, M. H. Leveraging Nanocavity Harmonics for Control of Optical Processes in 2D Semiconductors. *Nano Lett.* **2015**, *15* (5), 3578−3584.
(34) Wang, Z.; Dong, Z.; Gu, Y.; Chang, Y.-H.; Zhang, L.; Li, L.-J.; Zhao, W.; Eda, G.; Zhang, W.; Grinblat, G.; et al. Giant Photoluminescence Enhancement in Tungsten-Diselenide−gold Plasmonic Hybrid Structures. *Nat. Commun.* **2016**, *7*, 11283.
(35) Zhao, P.; Amani, M.; Lien, D.-H.; Ahn, G. H.; Kiriya, D.; Mastandrea, J. P.; Ager, J. W.; Yablonovitch, E.; Chrzan, D. C.; Javey, A. Measuring the Edge Recombination Velocity of Monolayer Semiconductors. *Nano Lett.* **2017**, *17* (9), 5356−5360.
(36) Sokolnikoff, S. A.; Friis, H. T. *Antennas: Theory and Practice*; John Wiley & Sons, Ince.: New York, 1952.
(37) Fortuna, S. A.; Eggleston, M.; Messer, K.; Yablonovitch, E.; Wu, M. C. Electrically Injected nanoLED with Enhanced Spontaneous Emission from a Cavity Backed Optical Slot Antenna. In *Photonics Conference (IPC)*; IEEE, 2014; pp 158−159.
(38) Amani, M.; Lien, D.-H.; Kiriya, D.; Xiao, J.; Azcatl, A.; Noh, J.; Madhvapathy, S. R.; Addou, R.; Kc, S.; Dubey, M.; et al. Near-Unity Photoluminescence Quantum Yield in MoS2. *Science* **2015**, *350* (6264), 1065−1068.
(39) Huang, C.; Wu, S.; Sanchez, A. M.; Peters, J. J. P.; Beanland, R.; Ross, J. S.; Rivera, P.; Yao, W.; Cobden, D. H.; Xu, X. Lateral Heterojunctions within Monolayer MoSe 2 − WSe 2 Semiconductors. *Nat. Mater.* **2014**, *13* (12), 1096−1101.